Modelling the effects of environmental heterogeneity within the lung on the tuberculosis life-cycle

Michael J. Pitcher[a], Ruth Bowness[b], Simon Dobson[a], Raluca Eftimie[c], Stephen H. Gillespie[b]

[a]*School of Computer Science, University of St Andrews*
[b]*School of Medicine, University of St Andrews*
[c]*School of Medicine, University of Dundee*

Abstract

Progress in shortening the duration of tuberculosis (TB) treatment is hampered by the lack of a predictive model that accurately reflects the diverse environment within the lung. This is important as TB has been shown to produce distinct localisations to different areas of the lung during different disease stages, with the environmental heterogeneity within the lung of factors such as air ventilation, blood perfusion and oxygen tension believed to contribute to the apical localisation witnessed during the post-primary form of the disease.

Building upon our previous model of environmental lung heterogeneity, we present a networked metapopulation model that simulates TB across the whole lung, incorporating these notions of environmental heterogeneity across the whole TB lifecycle to show how different stages of the disease are influenced by different environmental and immunological factors. The alveolar tissue in the lung is divided into distinct patches, with each patch representing a portion of the total tissue and containing environmental attributes that reflect the internal conditions at that location. We include populations of bacteria and immune cells in various states, and events are included which determine how the members of the model interact with each other and the environment. By allowing some of these events to be dependent on environmental attributes, we create a set of heterogeneous dynamics, whereby the location of the tissue within the lung determines the disease pathological events that occur there.

Our results show that the environmental heterogeneity within the lung is a plausible driving force behind the apical localisation during post-primary disease. After initial infection, bacterial levels will grow in the initial infection location at the base of the lung until an adaptive immune response is initiated. During this period, bacteria are able to disseminate and create new lesions throughout the lung. During the latent stage, the lesions that are situated towards the apex are the largest in size, and once a post-primary immune-suppressing event occurs, it is the uppermost lesions that reach the highest levels of bacterial proliferation. Our sensitivity analysis also shows that it is the differential in blood perfusion, causing reduced immune activity towards the apex, which has the biggest influence of disease outputs.

Keywords: Tuberculosis, Computational biology, Within-host model, Bacteria, Metapopulation, Lung, Localisation

Email address: mjp22@st-andrews.ac.uk (Michael J. Pitcher)

1. Introduction

Tuberculosis (TB) accounts for over 1 million deaths each year [1], despite the fact that an effective treatment has existed for decades. The current standard regimen for drug-susceptible forms of TB requires six months of multiple antibiotics, and a large number of factors can contribute to a patient's ability to adhere to the treatment [2]. Non-adherence can have serious consequences, both for the patient, as it increases the chances of relapse after treatment, and for the wider society, as an incomplete course of antibiotics can lead to the remaining bacteria developing drug resistance [3, 4]. Therefore, creating novel regimens of shorter duration is of great importance, as doing so would improve overall patient adherence and reduce these risks of relapse and drug resistance. Unfortunately, recent efforts to create new regimens of four months have not been successful.

Experiments on mice using moxifloxacin showed promising results with regard to bactericidal effects [5] and it was predicted that the use of this drug could reduce human treatment duration. However, clinical trials incorporating the drug in novel regimens were unable to prove non-inferiority [6, 7], possibly due to the heterogeneity of distribution of drugs within the lesion during treatment [8]. This demonstrates a crucial hurdle in the drug development process for TB: we lack the predictive power at the preclinical stage to make effective decisions as to which of the many possible new regimens to progress through to expensive and costly clinical trials. Using *in vitro* experiments, it is not possible the create the full environment seen within patients and there exists no single *in vivo* animal model which completely encapsulates the pathophysiology seen within humans [9]. *In silico* models, of both mathematical and computational form, could provide a compromise: allowing us to simulate the disease in a full (synthetic) environment at a fraction of the time and cost required for *in vitro* and *in vivo* models. The ability to create a simulation model that reflects the full spectrum of pathophysiology seen in humans with TB would reduce the use of animal models and allow us to make predictions as to the efficacy of novel regimens, and thus better inform our decisions with regard to prioritisation of these new treatments. Furthermore, the development of these models allows us to explore the dynamics of TB infection and provides insight into the complex dynamics that occur and which we do not fully understand yet.

TB infection begins with the inhalation of one or more *Mycobacterium tuberculosis* (*M. tuberculosis*) bacterium, which lands at the alveolar tissue of the lower respiratory tract, where it begins to replicate. There, a complex battle between the host immune response and the pathogen begins. Figure 1 shows the possible outcomes of a TB infection. In a small percentage of people, the immune response is sufficient and the bacterial load is low enough that the infection is cleared from the body. For most people, the bacteria proliferate and the innate immune response is insufficient to cope with the bacteria, and thus an adaptive immune response is triggered. In patients whose immune system is compromised in some manner, this adaptive immune response is also insufficient and thus active disease is formed, termed 'primary TB' as it originates from the initial bacterial load. In the majority of patients, the adaptive immune response is strong enough to contain but not eradicate the bacteria, and the infection remains in an asymptomatic 'latent' form. This latent form of disease represents a reservoir for bacteria, as the infection may re-activate if the immune system later weakens and the structures containing the bacteria suffer degradation, allowing the bacteria to replicate extracellularly. This is termed 'post-primary TB'.

Whilst both primary and post-primary stages are active, symptomatic forms of TB which can lead to patient mortality, it is important to recognise that these two forms of disease are distinct in localisation and pathology [11]. The initial infection site for TB tends to occur in the lower

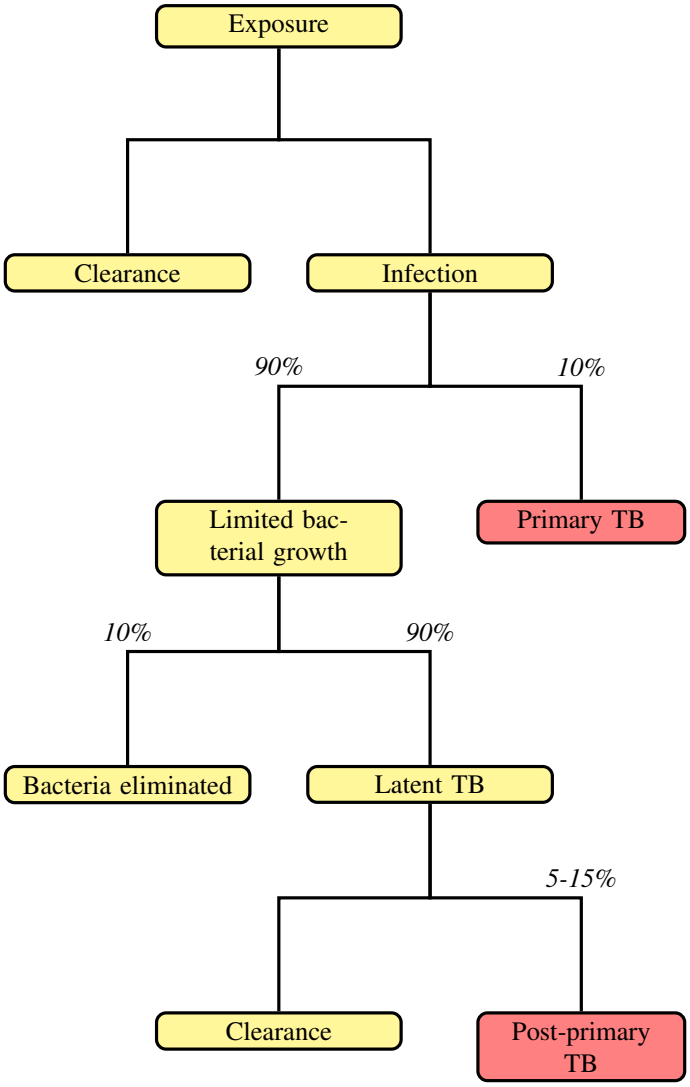

Figure 1: Overview of the clinical outcomes of *M. tuberculosis* exposure. Adapted from [10], values from [1, 10]. Red boxes indicate active, symptomatic disease.

regions of the lung, which are more ventilated than other lung regions. Post-primary disease involves cavitation, whereby the alveolar tissue is eroded and access is permitted to the bronchial tree, and this cavitation always occurs at the apices of the lungs [12]. Cavitation does not occur during primary disease. Thus, the bacteria that land in the lower regions must somehow disseminate to the apical regions, and the environment at the apex of the lungs must be preferential for cavitation to occur. It has been hypothesised that the environmental conditions within the lung contribute to these differences in localisation [12, 13, 14, 15], with factors such as the lower blood perfusion and higher oxygen tension at the apices compared to the basal regions believed to contribute to *M. tuberculosis* proliferation there. But exactly how these factors influences disease is not well understood.

In silico modelling of TB is still in its infancy, and most existing models of the disease have simulated the disease on the scale of a single lesion [16, 17, 18]. In [19], we presented the first *in silico* model of TB over the whole lung to incorporate the environmental heterogeneity present within the organ in order to understand how the differentials in factors such as blood perfusion and oxygen tension impact disease. In this paper, we build upon this model and present a new iteration of the model which includes a more granular network as its base and incorporates the full life-cycle of disease, to show how the environment within the lung impacts each stage of disease in a unique manner.

2. Whole lung model of TB with environmental heterogeneity

The model, termed *TBMetapopPy*, simulates the interaction between immune cells, bacteria, and the local environment both within the lung and in the associated lymphatics. It takes the form of a networked metapopulation: multiple patches exist within the model, which are linked together with edges to form a network. Patches contain subpopulations of various immune cells or bacteria, which may interact with each other and the local environment within the patch, or may translocate from one patch to another.

2.1. Environment

The spatial domain of the model consists of the alveolar tissue within the lung and the lymph nodes draining the lungs. The lung tissue is divided into multiple patches, each representing the total alveolar tissue present in a branch of the bronchial tree. Each patch within the lung contains environmental attributes that reflect the initial conditions within the lung at that position. These are listed in Table 1. As V and Q represent fractions of the total ventilation and perfusion, respectively, supplied to the lung that reach a patch, the sum of each of these values across all patches equals 1. The lymphatic patch contains no environmental attributes.

All patches contain populations divided into compartments, each of which represents the species and status of immune cells or bacteria, as described in Table 2. We model 4 types of bacteria, based on their location and/or replication rate. Bacteria that are present in or on the tissue surface are 'extracellular'. *M. tuberculosis* has been shown to exhibit 'dormancy', associated with the accumulation of lipid bodies, whereby it reduces its replication rate but becomes more resistant to antibiotics [20, 21]. In order to incorporate this, we allow bacteria to switch between a 'replicating' (B_{ER}) and a 'dormant' (B_{ED}) state when extracellular. *M. tuberculosis* has evolved to suppress the destructive mechanism of immune cells by preventing phagolysosome biogenesis, and thus is able to reside within the intracellular matrix of host cells [22, 23, 24]. We define two types of intracellular bacteria - those within dendritic cells (B_{ID}) and those inside macrophages

Label	Attribute	Description
V	Ventilation	The fraction of inhaled air that is passed to that area of the lung
Q	Perfusion	The fraction of all blood sent to the lung that reaches the given patch
O	Oxygen tension	Oxygen tension remaining in the air of the lungs after gas exchange has occurred. This is dependent on both the amount of air received (V) and the amount of blood received (Q).
G	Drainage	The rate at which cells are able to transfer from the lung to the lymphatics system relative to the lung average.

Table 1: Environmental attributes within the lung patches of *TBMetapopPy*

Label	Compartment
B_{ER}	Bacterium extracellular - replicating
B_{ED}	Bacterium extracellular - dormant
B_{ID}	Bacterium intracellular - dendritic
B_{IM}	Bacterium intracellular - macrophage
D_I	Immature dendritic cell
D_M	Mature dendritic cell
M_R	Resting macrophage
M_I	Infected macrophage
M_A	Activated macrophage
T_N	Naïve T cell
T_A	Activated T cell
C	Caseum

Table 2: Population compartments within TBMetapopPy

(B_{IM}), as both of these cells have been shown to become infected by *M. tuberculosis* [25]. We do not make the distinction between replicating and dormant here: we assume that dendritic cells are too small to permit internal bacterial replication, and that the internal environment within a macrophage is hostile and thus forces the bacteria into a slower-replicating state regardless of replication rate when ingested.

We model 3 types of immune cells: dendritic cells, macrophages and T cells. The primary role of dendritic cells in the model is antigen-presentation: the immature dendritic cells (D_I) resident in the lung encounter and ingest bacteria, causing them to convert to a mature state (D_M). These mature cells can then trigger an adaptive immune response by transferring to the lymphatics and activating T cells there. Macrophages play a similar role, as they can also encounter and ingest bacteria and transfer to the lymphatics, but we assume that macrophages are less mobile than dendritic cells and have a greater internal capacity - they are more likely to remain in the lung and attempt to eliminate bacteria there. Thus, macrophages have a 'resting' (M_R) and 'infected' state (M_I). We also include an 'activated' state (M_A), whereby the macrophage's bactericidal ability is improved during an adaptive immune response [26].

Symbol	Description	Value
P	A series of (x,y) coordinates composing the external perimeter of the model environment	(50,0), (0, 0), (0, 100), (50, 100)
a	An (x,y) point, on P, where the branching process originates from	(50, 50)
f	The length of the new branch as a fraction of the line dividing the perimeter in two	2
z	The minimum area needed to stop the branching process	0.05
S_V	The skew of ventilation values from base to apex, i.e. how many times greater the V value will be for a patch at the very base of the lung compared to one at the very apex of the lung	2
S_Q	The skew of perfusion values from base to apex	3
S_G	The skew of drainage values from base to apex	1

Table 3: Parameters for constructing the environment of *TBMetapopPy*

Naïve T cells (T_N) are present within the lymphatic system and may be activated by antigen-presenting cells. Multiple varieties of activated T cells exist within the lungs with varying different functions [27, 28]. For simplicity, we do not make a distinction between the different roles and include just one type of activated T cell (T_A) to serve as a representation for all real-world types.

2.2. Initial conditions

At the start of a simulation using *TBMetapopPy*, a network is constructed, using the parameters in Table 3, which models the bronchial tree as a simple space-filling tree. Firstly, a set of coordinates which define the perimeter, P, are provided, creating a two-dimensional shape, S. A point, a, on the perimeter is also chosen. The following algorithm is then executed to build a space-filling tree:

1. A point, b, on P is chosen such the line ab bisects the shape S evenly
2. A point, c, is created on the line ab, whereby the line ac is a fraction, f, of the distance of the line ab.
3. Steps 1 and 2 are repeated twice, this time using c as the start point and perimeter series of $c-a-P_1-b-c$ and $c-b-P_2-a-c$ respectively, where P_1 represents the points between a and b on perimeter P, and P_2 is the points from b back to a.
4. Each iteration creates two new shapes of half the size of the parent shape. A threshold, z, is provided, and once the child shape sizes drop below this threshold, the iteration at that branch terminates.
5. The endpoints of the branch form the patches of the finished network.

This process (an example of which is shown in Figure 2) creates a space-filling tree: the end points of the tree may be geometrically close to one another but distant on the bronchial tree. A further patch is added to represent the lymphatic system. In order to create a network, edges are added to show translocation of members across the system. An edge is added between every alveolar patch and the lymph patch.

Once constructed, the environment is firstly seeded with values for the environmental attributes of the lung patches. Ventilation skew (S_V) and perfusion skew (S_Q) parameters are defined such that a patch at the very apex of the lung would have both V and Q values set to 1, whilst a patch at the very base of the lung would have a V value of S_V and Q value of S_Q.

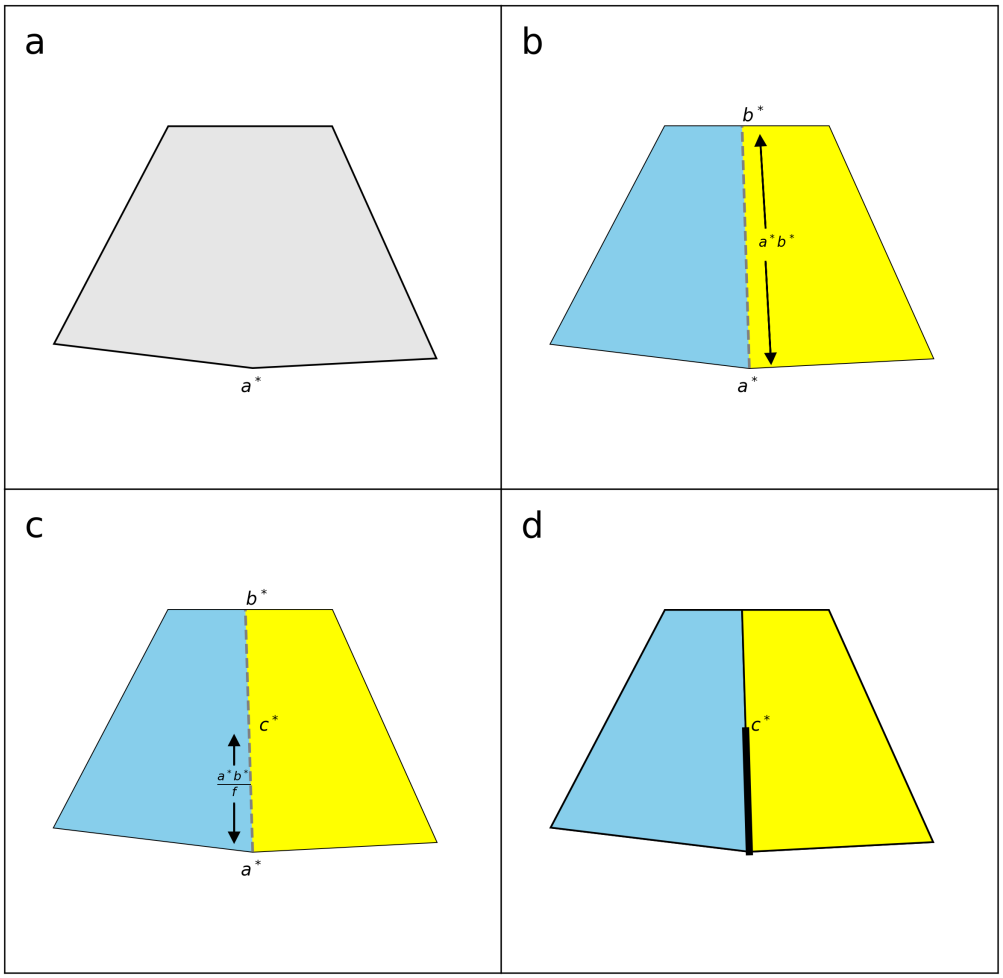

Figure 2: Example of the branching algorithm used to generate the environment within the second *TBMetapopPy* model.

Patches are then assigned values according to these scales and based on their vertical position, as shown in Equations 1 and 2, where y is the vertical position of the patch, y_{max} is the y-coordinate of the highest vertical point of the area and y_{min} is the y-coordinate of the lowest vertical point. These equations create linear scales of perfusion and ventilation across the lung, as seen in the literature [29].

$$V = 1 + (y_{max} - y) * \frac{S_V - 1}{y_{max} - y_{min}}, \tag{1}$$

$$Q = 1 + (y_{max} - y) * \frac{S_Q - 1}{y_{max} - y_{min}}. \tag{2}$$

Once every patch in the lung has been assigned these values, the sums of all V and Q are calculated and each patch's values are divided by these totals in order to normalise them and ensure the sum of all values across the lung comes to 1. Oxygen tension, O, is calculated automatically as per Equation 3.

$$O = \frac{V}{Q} \tag{3}$$

All patches (lung and lymph) are then seeded with population values. Lung patches are assumed to contain M_R and D_I in the absence of infection, with the lymph patch containing M_R and T_N. We assume these populations remain at an equilibrium level without infection calculated as per Equation 4, where C_x is the equilibrium value for the compartment x, R_x is the recruitment rate for x and μ_x is the death rate for x.

$$C_x = \frac{R_x}{\mu_x}. \tag{4}$$

Within the lung, the recruitment rate for a given compartment will be scaled by the perfusion, Q, at the patch, resulting in Equation 5.

$$C_x = \frac{QR_x}{\mu_x}. \tag{5}$$

Finally, bacteria are seeded within the lung, with loads of I_R for B_{ER} and I_D for B_{ED} placed within a single patch in the lung. The choice of patch can either be chosen randomly based on ventilation values or hard-coded to a specific patch dependent on the scenario being explored.

2.3. Events

As the simulation runs, populations are able to interact with each other and the local environment, with members switching into different compartments as they change states or locations. Here, we define the dynamics that occur within the *TBMetapopPy* model. The event system of the model uses the Gillespie Algorithm to model time - each interaction is coded as a separate event and each must define how its rate of occurrence is calculated from the event parameters (listed in Table 4 and explained in Section 2.4) and the current population counts of the network, and must also define the outcome of the event being performed.

2.3.1. Innate immune response

M_R cells are initially present in both the lung and lymphatic system. These cells die naturally at a rate of μ_{MR}, and are replaced through recruitment which occurs at rate $Q\alpha_{ML}$ in the lung and α_{MY} in the lymph. As Q is the perfusion value at the patch, which is itself a fraction of the perfusion to the whole lung, the parameter α_{ML} represents the total number of cells recruited to the entire lung, a portion of which will be sent to a specific patch.

D_I cells also die (at rate μ_{DI}), and are replaced in the lung through recruitment (at rate $Q\alpha_D$). In the lymphatics, naïve T cells die (at rate μ_{TN}) and are replaced through recruited cells (at rate α_T).

The bacteria in the lung are initially extracellular and are able to replicate freely, with B_{ER} replicating at rate $\lambda_R B_{ER}$ and B_{ED} replicating at rate $\lambda_D B_{ED}$. In order to model the effects of hypoxia on bacterial replication, we include an event to switch bacteria to B_{ED} with increased likelihood in an oxygen-poor environment, with rate $\xi B_{ER}\Big(\frac{O^{-\sigma_\xi}}{O^{-\sigma_\xi}+\theta_\xi{}^{-\sigma_\xi}}\Big)$, whereby $\sigma_\xi > 0$. We also include the reverse event, with B_{ED} converting to B_{ER} when presented with an oxygenated area, with rate equal to $\xi B_{ED}\Big(\frac{O^{\sigma_\xi}}{O^{\sigma_\xi}+\theta_\xi{}^{\sigma_\xi}}\Big)$.

The phagocytes within the lung may encounter the bacteria and ingest them. This occurs at rate $\gamma_R M_R \frac{B_E}{B_E+\theta_{\gamma R}}$ for M_R and rate $\gamma_D D_I \frac{B_E}{B_E+\theta_{\gamma D}}$ for D_I, where $B_E = B_{ER} + B_{ED}$. When performed, an extracellular bacteria is probabilistically chosen to be ingested based on current levels. We model the ability of *M. tuberculosis* to avoid destruction by assigning a probability to bacterial destruction when M_R encounter bacteria, with η representing the probability that a M_R cell will become infected and the bacterium will become intracellular , whilst $(1-\eta)$ represents the probability that the bacterium will be destroyed. We assume that D_I are incapable of bacterial destruction and so always convert to D_M when ingesting bacteria, and that the different replication phenotypes (B_{ER} or B_{ED}) have the same chances of survival under phagocytosis.

If a bacteria survives the ingestion process, it converts to an intracellular state (B_{IM} or B_{ID} for phagocytosis by M_R or D_I respectively) and the cell converts to an infected state (M_R convert to M_I, D_I convert to D_M). M_I and D_M both die naturally, at rates $\mu_{MI} M_I$ and $\mu_{DM} D_M$ respectively, and this may return some of the internal bacteria back into extracellular compartment B_{ED} (we assume that the internal conditions within a macrophage are stressful to bacteria and thus they have been forced into a dormant state, which they remain in once released). For D_M death, we assume the single internal B_{ID} is always released, whilst for M_I death, we assume a percentage of the bacteria inside the macrophage ($\psi_\mu \frac{B_{IM}}{M_I}$) are destroyed with the remainder ($(1-\psi_\mu)\frac{B_{IM}}{M_I}$) released.

Once in the internal compartment of the immune cell, bacteria can replicate, constrained by the internal capacity of the cell. We assume D_I cells are too small to permit replication and thus B_{ID} do not replicate. B_{IM} may replicate at rate $\lambda_I B_{IM}\Big(1-\frac{(B_{IM})^{\sigma_\lambda}}{(B_{IM})^{\sigma_\lambda}+(\phi M_I)^{\sigma_\lambda}}\Big)$. Thus the rate of replication decreases as the levels of bacteria approach the total carrying capacity of all infected macrophages (ϕM_I). As macrophages start to fill with bacteria, they may 'burst', rupturing their outer wall and releasing bacteria. The rate of occurrence for this is inverse to replication, i.e. it increases as the bacterial level approaches capacity, with rate $\beta M_I\Big(\frac{(B_{IM})^{\sigma_\lambda}}{(B_{IM})^{\sigma_\lambda}+(\phi M_I)^{\sigma_\lambda}}\Big)$. When this occurs, a fraction of total B_{IM} (calculated as $\psi_\zeta \frac{B_{IM}}{M_I}$) are destroyed, with the remainder, $(1-\psi_\zeta)\frac{B_{IM}}{M_I}$, returning to the compartment B_{ED}. The death of an infected macrophage releases a portion of caseum, C, into the extracellular compartment.

Resting macrophages may overcome their inability to destroy bacteria by activating - this converts the M_R member to M_A. This process is triggered by the presence of bacteria, at rate $\epsilon_{MB} M_R \frac{B_E}{B_E+\theta_{\epsilon MB}}$. Activated macrophages can ingest bacteria in the same manner as M_R, with rate $\gamma_A M_A \frac{B_E}{B_E+\theta_{\gamma A}}$, but M_A cannot become infected and thus the bacteria ingested are always destroyed, simulating the increased bactericidal effects of macrophage activation. M_A cells die at rate $\mu_{MA} M_A$.

Infection is not just restricted to the initial location and the lymphatics. We assume that there exists a period of time after bacteria become present in the lymphatics and before the

establishment of a structured lesion there, and that during this time period bacteria are able to freely move from the lymph nodes into the blood and thus be transferred back into the lung to seed new lesions. In modelling terms, we assume that the presence of caseum indicates a stable lesion, and thus the rate of translocation of bacteria from the lymphatics into the lung is $\tau_{BY} B_{ED}(1 - \frac{C}{C+\theta_{\tau BY}})$.

2.3.2. *Adaptive response*

In response to infection, the body increases the supply of immune cells to the lung to assist within containment. This is modelled by separate events for each resident immune cell type at each location. In the lung, enhanced macrophage recruitment occurs at rate $\beta_{ML} Q \frac{\omega M_I + M_A}{\omega M_I + M_A + \theta_{\beta ML}}$. We assume that M_I and M_A cells create the necessary chemokines to trigger enhanced recruitment, and include ω as a weighting term to allow for these cells to produce differing levels of chemokine. Similarly, dendritic cell recruitment is enhanced at rate $\beta_D Q \frac{\omega M_I + M_A}{\omega M_I + M_A + \theta_{\beta D}}$. In the lymphatics, macrophage recruitment is enhanced at rate $\beta_{MY} \frac{\omega M_I + M_A}{\omega M_I + M_A + \theta_{\beta MY}}$. Enhanced T cell recruitment is dependent on dendritic cells and is increased at rate $\beta_T \frac{D_M}{D_M + \theta_{\beta T}}$.

Both dendritic cells [30, 31] and macrophages [32] have been shown to transfer to the lymphatics during infection in order to present antigens and trigger an adaptive immune response. We treat both D_I and M_I as antigen-presenting cells and we model their transfer to the lymphatics as two separate events: with D_I translocating at rate $\tau_D G D_I$ and M_I translocating at rate $\tau_M G M_I$, thereby creating different rates of clearance at different regions, based on G. This transfer, whilst necessary for establishing an adaptive immune response, also carries the risk of spreading infection, as any internalised bacteria are also transferred to the lymphatics. The transfer of bacteria to the lymph nodes may be a necessity for establishing an adaptive immune response [33]. Thus in our model, transfer of M_I also causes the transfer of B_{IM} members (calculated as the average number of B_{IM} per M_I), and transfer of a D_M member also transfers a single B_{ID}.

Antigen-presenting cells in the lymphatics can cause activation of T cells from a naïve to an activated state. This occurs at rate $\epsilon_T T_N \frac{M_I + D_M}{M_I + D_M + \theta_{\epsilon T}}$, and results in T_N changing to T_A. Once activated, these T cells migrate to the sources of infection to enhance the immune response and contain the bacteria. We allow the body to direct T cells to where they are needed by basing the rate of translocation of these cells from the lymphatics to the lung on the number of D_M - the presence of these cells in the lymphatics gives an indication of the level of infection within the lung as they only originate within the lung. Thus, increased numbers of D_M in the lymphatics indicates that more T cells need to migrate to contain infection in the lung, rather than remaining in the lymph to fight infection there. The rate of translocation is $\tau_T T_A \frac{D_M}{D_M + \theta_T}$.

Activated T cells perform two primary functions in the model: the first is to cause activation of macrophages, converting M_R into M_A, occurring at rate $\epsilon_{MT} M_R \frac{T_A}{T_A + \theta_{\epsilon MT}}$. The second function of T_A is to causes apoptosis - the controlled destruction of infected cells. This is modelled by allowing T_A members to destroy M_I members at rate $\kappa_M M_I \frac{T_A}{T_A \theta_{\kappa M}}$. Doing so also destroys some internal bacteria, calculated as $\psi_{\kappa M} \frac{B_{IM}}{M_I}$, with $(1 - \psi_{\kappa M}) \frac{B_{IM}}{M_I}$ converting from B_{IM} to B_{ED}. T_A members naturally die at rate $\mu_{TA} T_A$.

2.3.3. *Weakening of the immune system*

The events described previously constitute the primary and latency stages of infection: an initial infection occurs within the lungs and the bacteria levels are brought under control by an adaptive immune response. In order to model a post-primary infection (more specifically, a reactivation scenario whereby the immune system containing the bacteria during the latency

Parameter	Description	Baseline	Dist.	Range	Ref
λ_R	B_{ER} replication rate	0.814	N	0.03	[16]
λ_D	B_{ED} replication rate	0.26	N	0.01	[16]
λ_I	B_{IM} replication rate	0.26	N	0.01	E
σ_λ	Sigmoid for B_{IM} replication	2.0	N	0.01	[34]
ϕ	Carrying capacity of macrophages	50	N	10	[34]
ξ	Rate of conversion between bacterial states	1	U	0.01 - 2.0	E
θ_ξ	Half-saturation for conversion between bacterial states	1	U	0.01 - 2.0	E
σ_ξ	Sigmoid for conversion between bacterial states	2	U	1.0 - 3.0	E
τ_{BY}	Rate bacteria move from lymphatics to lung	1e-3	U	5e-4 - 2e-3	E
$\theta_{\tau BY}$	Half-sat of caseum stopping bacterial reseeding of lung	500	U	250 - 750	E
α_D	Rate of standard recruitment of D_I into the lung	599e4	N	75e4	E
β_D	Rate of enhanced recruitment of D_I into the lung	5000.05	U	1e-1 - 1e5	E
$\theta_{\beta D}$	Half-sat value for enhanced recruitment of D_I in lung	5500	U	1e3 - 1e4	E
μ_{DI}	Death rate of D_I	0.01	N	4e-3	[34]
μ_{DM}	Death rate of D_M	0.3	N	0.1	[34]
γ_D	Rate at which D_I encounters bacteria	0.3	U	0.2-0.4	E
$\theta_{\gamma D}$	Half-sat value for contact between D_I and bacteria	5500	U	1e3 - 1e4	E
τ_D	Rate of translocation of D_M from lung to lymphatics	0.55	U	0.1 - 1.0	[35, 36]
α_{ML}	Rate of standard recruitment of M_R into the lung	599e5	N	75e5	[37]
β_{ML}	Rate of enhanced recruitment of M_R into the lung	50000.05	U	1e-1 - 1e5	E
$\theta_{\beta ML}$	Half-sat value for enhanced recruitment of M_R in lung	5e3	U	1 - 1e4	E
α_{MY}	Rate of standard recruitment of M_R into the lymphatics	53.465	N	3.0	[35]
β_{MY}	Rate of enhanced recruitment of M_R into lymphatics	750	U	600 - 900	E
$\theta_{\beta MY}$	Enhanced recruitment of M_R in lymph half-sat	5500	U	1e3 - 1e4	E
ω	Weighting value for chemokine release by M_I to M_A	0.55	U	1e-2 - 1	E
μ_{MR}	Death rate of M_R	0.01	N	4e-3	[34]
μ_{MA}	Death rate of M_A	0.01	N	4e-3	[34]
μ_{MI}	Death rate of M_I	0.01	N	4e-3	[34]
ζ	Rate of bursting of M_I	0.25	N	0.05	[34]
τ_M	Rate of migration of M_I from lung to the lymphatics	0.001	U	1e-4 - 1e-1	E
ϵ_{MB}	Rate of activation of M_R by extracellular bacteria	0.01	U	1e-4 - 1e-1	E
$\theta_{\epsilon MB}$	Half-sat for activation of M_R by extracellular bacteria	5500	U	1e3 - 1e4	E
ϵ_{MT}	Rate of activation of M_R by T_A	0.3	U	0.1 - 0.5	[34]
$\theta_{\epsilon MT}$	Half-saturation for activation of M_R by T_A	5500	U	1e3 - 1e4	E
κ_M	Rate at which T_A destroy M_I	1.35	U	0.7 - 2	[34]
$\theta_{\kappa M}$	Half-saturation value for T_A destruction of M_I	1e3	U	1e1 - 2e3	E
$\psi_{\kappa M}$	% of bacteria destroyed when M_I is destroyed by T_A	0.5	U	0.5 - 1	E
γ_R	Rate at which M_R ingest bacteria	0.3	N	0.01	[34]
$\theta_{\gamma R}$	Half-sat for contact between M_R and bacteria	5500	U	1e3 - 1e4	E
η	Probability M_R becomes infected during phagocytosis	0.75	U	0.5-1.0	E
γ_A	Rate at which M_A ingest bacteria	0.8	U	0.2-1.4	E
$\theta_{\gamma A}$	Half-sat for contact between M_A and bacteria	5500	U	1e3 - 8e3	E
α_T	Rate of standard recruitment of T_N into lymphatics	1000	N	3.0	[34]
β_T	Rate of enhanced recruitment of T_N into lymphatics	1000	U	900 - 4000	E
$\theta_{\beta T}$	Enhanced recruitment of T_N into lymphatics half-sat	1e3	U	1 - 2e3	E
ϵ_T	Rate of activation of t-cells	0.4	U	0.1 - 0.7	[34]
$\theta_{\epsilon T}$	Half-sat value for activation of T cells	1e3	U	1e1 - 2e3	E
τ_T	Rate of T cell migration from lymphatics into lung	0.625	U	0.3 - 0.95	[34]
σ_T	T cell migration sigmoid	0.25	U	1e-3 - 3.0	E
μ_{TN}	Rate of death for T_N	0.102	N	1e-2	[34]
μ_{TA}	Rate of death for T_A	0.333	N	1e-2	[34]
λ_T	Rate of replication for T_A	0.15	U	1e-3 - 0.3	E

Table 4: Event parameters (E = estimated). All values are based on rates of event per day.

phase is compromised and thus allows for bacterial levels to rise again), we include an event that reduces the rate of T cell recruitment (i.e. α_T is decreased). Unlike the previous events, this event is not stochastic and instead is coded to occur at a user-defined time-point. For or experiments, we chose for this event to occur at 350 days, after latency has been established and the bacterial loads have relatively stabilised.

2.4. Parameters

The parameters used in the event dynamics, environment construction and initial conditions are listed in Table 4, and have been derived from existing literature where possible or estimated. Each parameter is given a baseline value for the purposes of running individual simulations (see Section 3), as well as a range, representing the biological uncertainty of the parameter, which is used for sensitivity analysis (see Section 4).

3. Results

We began by running simulations using the model with parameters set to the baseline values as defined in Tables 3 and 4. As the model is stochastic, 32 repetitions were run and the results presented are averaged over these repetitions.

3.1. Primary infection to latent infection - total bacteria and lesion size

We first examined the total bacterial load of the system over time. Figure 3 shows the results of the total bacterial load for each of the 32 repetitions over time. In the initial phase, a primary infection begins and reaches its peak between 25 and 45 days in all simulations. This is brought under control by the introduction of the adaptive immune response with low bacterial levels in all simulations by about day 55. This correlates with evidence that the adaptive immune response for TB occurs within humans within 5-6 weeks [36].

Whilst all simulations are relatively consistent to the point where the infection has been brought under control, with only minor variations in the height and time of the peak of initial infection, the results vary much greater in the response after this point. Whilst many simulations tend to keep bacteria numbers at a low level, for those that do not, the total number present has a large amount of variation. But it is impossible from this Figure to accurately understand the whole situation: a high bacterial load may be a result of a single large lesion, or multiple small lesions. It is important to make the distinction between these two scenarios: multiple small lesions can be interpreted as being stable: the immune system is able to keep these lesions at a low level and stop bacterial growth; whereas a large lesion can be interpreted as a failure of the immune system to control bacterial growth at that location: this may lead to tissue damage, and then cavitation. Therefore, it is preferable for the host to keep the lesion size small, and it is important for us to understand the size of the lesions created. We investigated the notion of bacteria distribution by tracking the average size of all lesions for each simulation, with the results shown in Figure 4. Here, we see that the average lesion size after day 60 is much lower: indicating that while there are a high number of bacteria, they are often being contained in multiple smaller lesions than fewer, tissue-damaging large lesions.

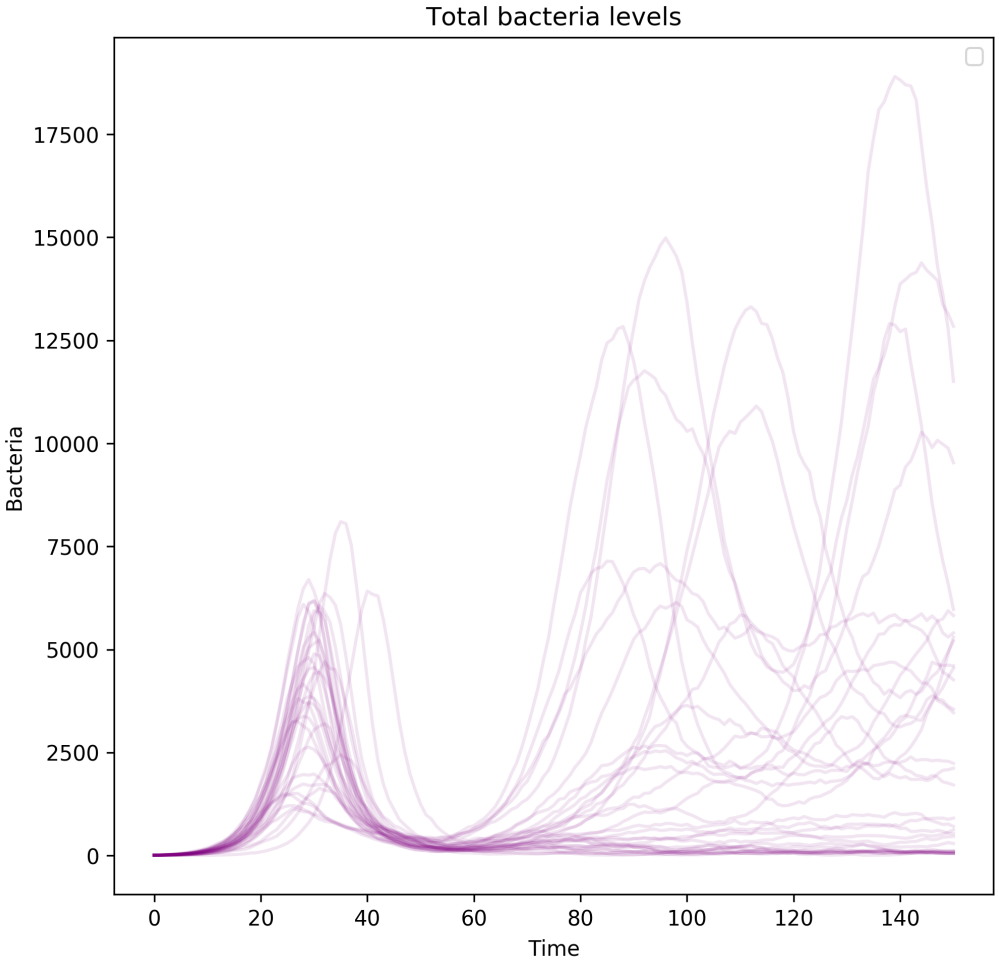

Figure 3: Total bacterial load of all patches over time within the *TBMetapopPy* system, showing individual counts for each of 32 repetitions

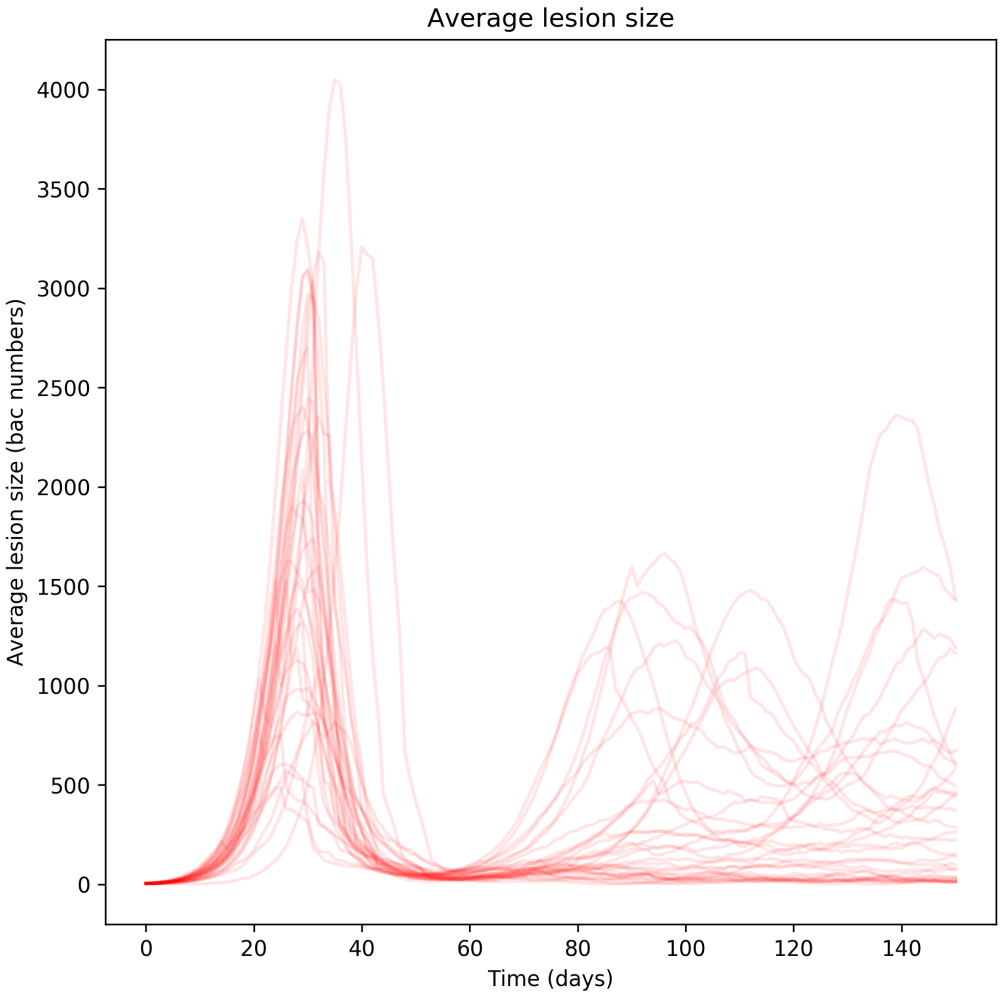

Figure 4: Average size (measured as number of bacteria) of all lesions over time within the *TBMetapopPy* system, showing individual averages for each of 32 repetitions

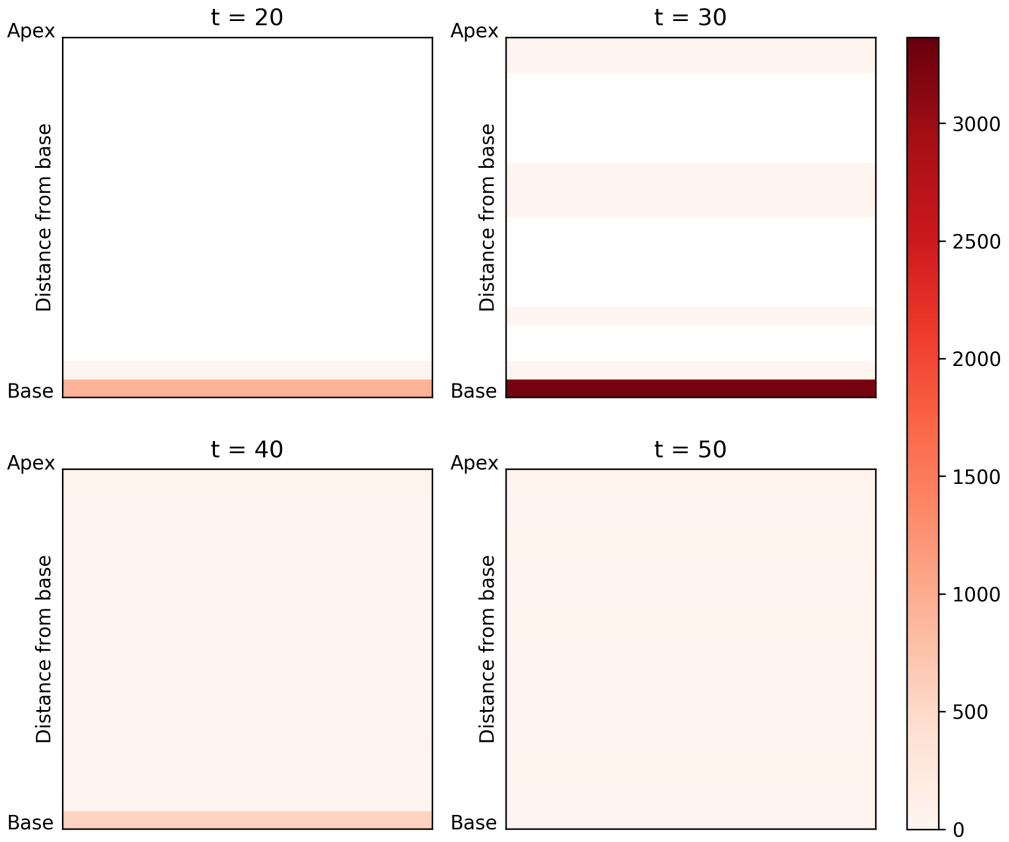

Figure 5: Vertical distribution of lesion sizes with *TBMetapopPy* simulations during the primary infection stage. Colour shows the average lesion size at each of 20 evenly sized horizontal slices of lung taken from 32 simulations.

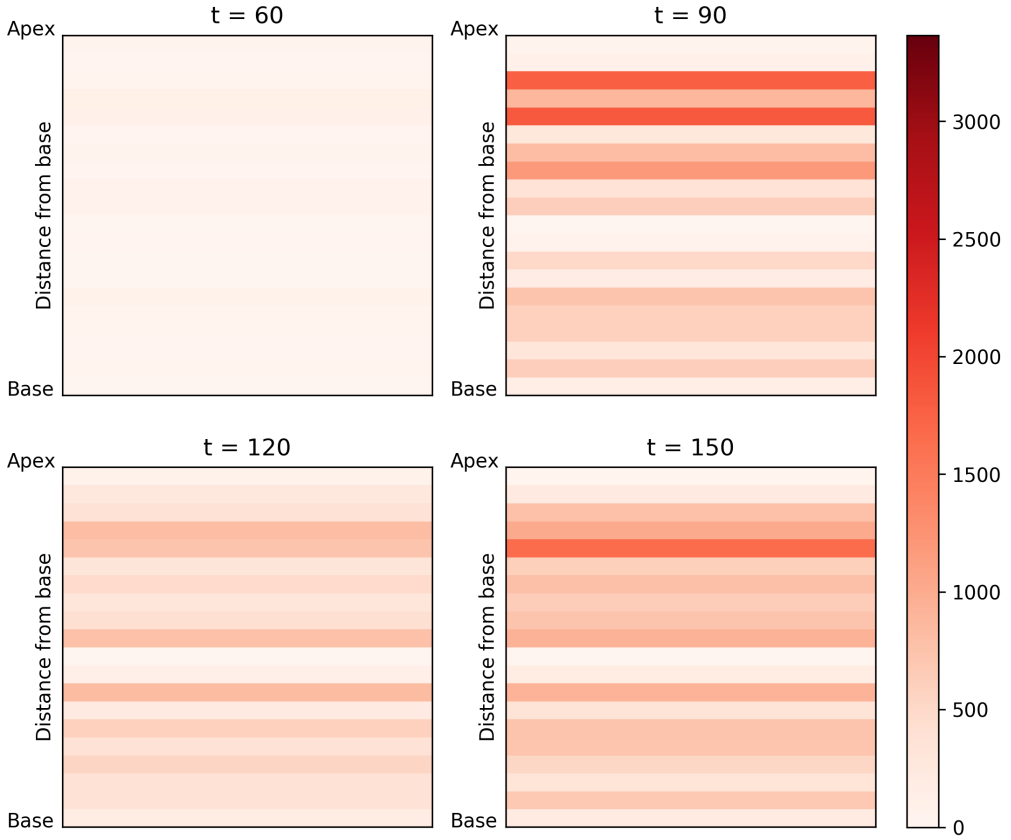

Figure 6: Vertical distribution of average lesion sizes with *TBMetapopPy* simulations during the latent infection stage

3.2. Spatial distribution of lesions and lesion size from primary to latent infection

We then explored which spatial areas of the lung were being affected by the disease over the course of the infection, by looking at the average lesion size for each horizontal slice of alveolar tissue (i.e. we group patches together that fall within the same given vertical position boundaries). Figure 5 shows the correlation of average lesion size to vertical position in the lung during the primary stages of infection. The initial lesion (in the very lowest region) grows and peaks at around 30 days - this was the largest average lesion size seen over the whole course of the simulation time-frame. By day 50, the lesion has stabilised but bacteria have spread to other regions of the lung. At this point, these lesions are all at a very small average size, despite the differences in their life-cycles: the large, older lesion at the base has almost completely healed, whilst the lesions at other regions in the lung have just begun and are thus at a small size. Figure 6 shows the average lesion size during the following stages of infection, from day 60 to day 150. We witnessed that whilst lesion size starts homogeneous across the lung, as time progresses the lesions at the apical region start to expand at a greater rate than those towards the base. This is in stark contrast to the lesions during the primary stage, which are typically completely homogeneous in terms of bacterial load. The size of these lesions during latency fluctuates in

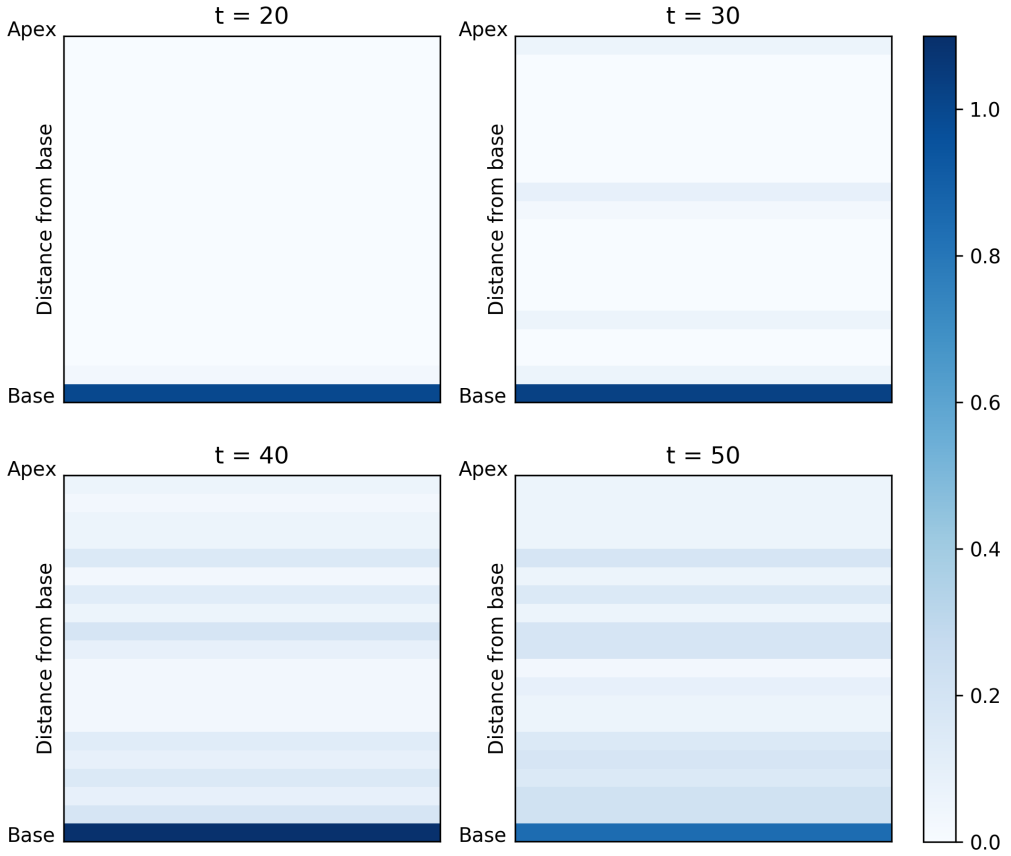

Figure 7: Vertical distribution of the number lesions with *TBMetapopPy* simulations during the primary infection stage

a sinusoidal manner (see Figure 4), but these average lesions sizes never reach the size seen during the primary infection. We further explored the numbers of lesions during infection, again stratifying the lesions based on their vertical position. Figure 7 shows the average number of lesions in each horizontal division of the lung per simulation. Here, we only counted patches where there was a bacterial presence - i.e. any lesions that were healed (no bacteria remaining) were not counted. In the primary stages, there is always a lesion present in the lowest basal region (the initial lesion where infection begins). By day 50, other lesions have begun to form across the lung, with a fairly even spread across the vertical dimension. Figure 8 shows the average number of lesions per horizontal section per simulation for later timesteps. At the very bottom section, the number of lesions decreases and reaches a level comparable to the rest of the lung. This occurs due to healing: the original lesion is, in many simulations, being completely healed of bacteria and thus is no longer counted. For the remainder of the lung, we witnessed some heterogeneity in the number of the lesions. By day 120, there appear to be two distinct regions with greater lesion counts: one at the very bottom of the lung and one in the second quadrant from the top of the lung (marked A and B respectively on Figure 8).

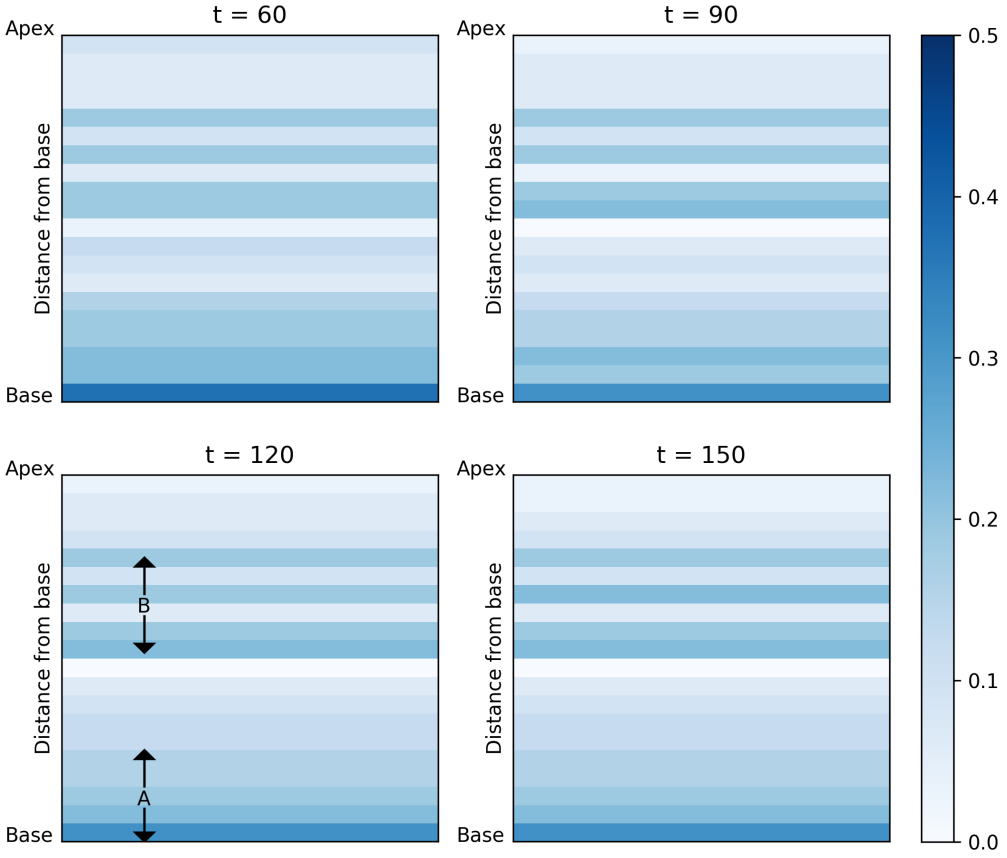

Figure 8: Vertical distribution of the number lesion sizes with *TBMetapopPy* simulations during the latent infection stage. Colour shows the average number of lesions present at each of 20 evenly sized horizontal slices of lung, with average taken from 32 simulations. A and B denote the regions with greatest number of lesions.

3.3. Post-primary disease

Having established that our model permits a higher bacterial load towards the apices during latent infection, we then proceeded to model the post-primary stage of the disease. As the actual causes of the change from latency to post-primary are unclear, and may not be the same for every individual case, we chose to model one case: a weakening of the immune system. In order to model this, we introduced a static event, which is set at the beginning of simulation and will always occur at the set time-point. This event drops the T cell recruitment rate, α_T, by half, and is set to occur at 250 days, well after latency has been established. We again ran 32 simulations, this time running for 500 days.

Figure 9 shows the distribution of the average lesion size for each of the 32 simulations. We see the same pattern as before for primary and latency disease. At the time of the T cell recruitment drop, the lesion sizes increase again, in many cases reaching levels similar to those seen at primary disease. We determine these to be a post-primary form of disease. We also note that not all replications reach this level: in some cases, where the average lesion size was low during latency, the average lesion size after the T cell recruitment drop increases but does not reach these high levels. In Figure 9 we show the spatial distribution of average lesion sizes within the lung. Again, the lesion size is large at base during primary infection (t=30), and this levels out at the end of primary infection and the beginning of the latent phase (t=60), with a slightly greater lesion size (approximately 1400) at the apex during latency (t=150). After the T cell recruitment drop, the average lesion sizes increase, with the largest (at approximately 3300 bacteria), most damaging lesions appearing at the apex of the lung (t=400).

4. Sensitivity Analysis

Having established that the environmental heterogeneity present within the lung environment can plausibly contribute to the differences in localisation seen during different stages of infection, we then proceeded to run uncertainty and sensitivity analysis, exploring the scale of uncertainty present within the results of our model and apportioning this uncertainty to the uncertainty within our input parameters. The reasons for doing this are two-fold. Firstly, our model, like any model constructed to simulate real-world biology, is built upon real-world data which is often incomplete [38], possibly due to a lack of available *in vivo* and *in vitro* models. Therefore, it is important to understand exactly how this uncertainty in the model input propagates to its outputs, as this can highlight which uncertain parameters should be investigated further (perhaps in a laboratory or clinical trial setting) in order to reduce the parameter uncertainty and thus improve our confidence in the model's outputs. Secondly, by varying the values of input parameters and tracking the variance of the model's outputs, we are afforded insight into which of the model parameters is most influential on the given output, and thus can deduce which individual events within the system most influence disease outcomes. Future treatments that can target these important functions would be more likely to be successful.

Our model contains a large number of parameters based on biological processes which are uncertain, and this introduces a large amount of uncertainty into our results. As these parameters drive various events within the model that rely on the same elements (such as the bacterial and immune cell compartments), it is reasonable to assume that there will be interactions between parameters. Furthermore, the complex host-pathogen interactions that occur during TB disease mean that we can expect non-linearities to be present in our model as well, as shown in our

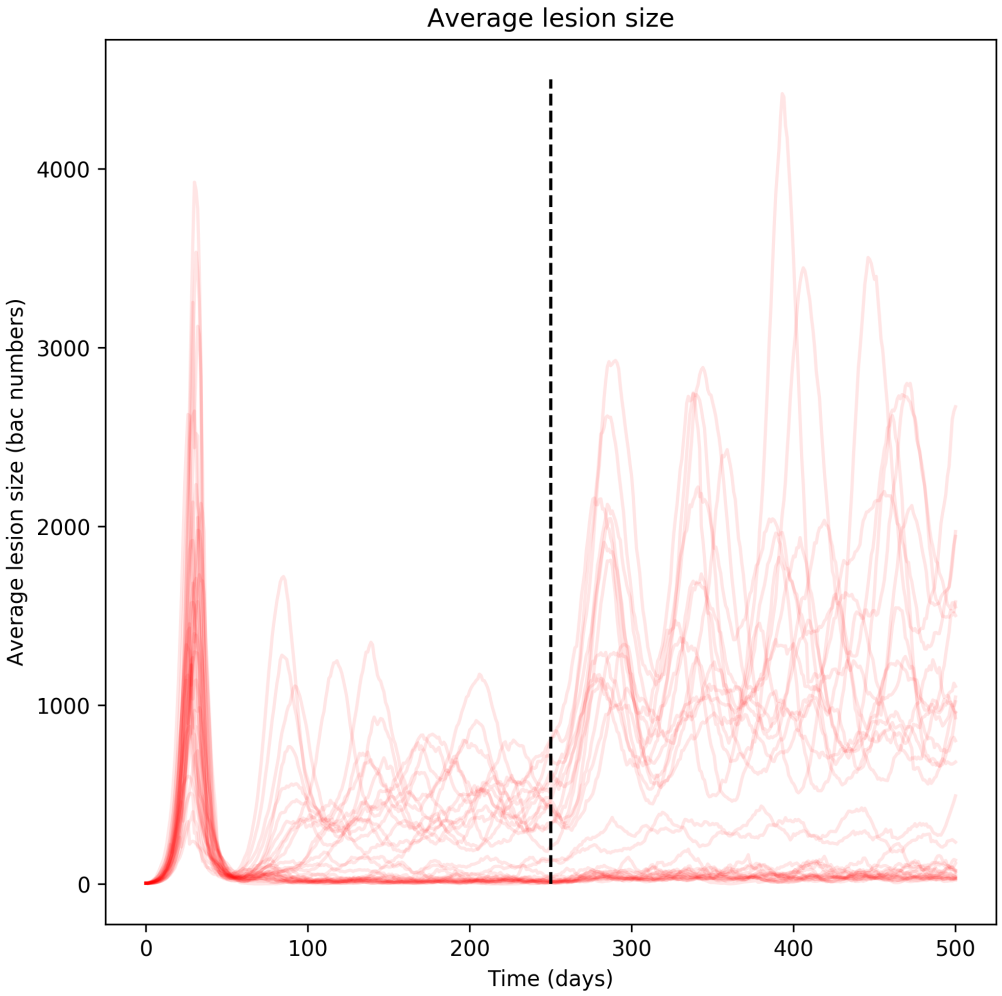

Figure 9: Average size (measured as number of bacteria) of all lesions over time within the *TBMetapopPy* system incorporating a T cell recruitment drop (black line), showing individual averages for each of 32 repetitions

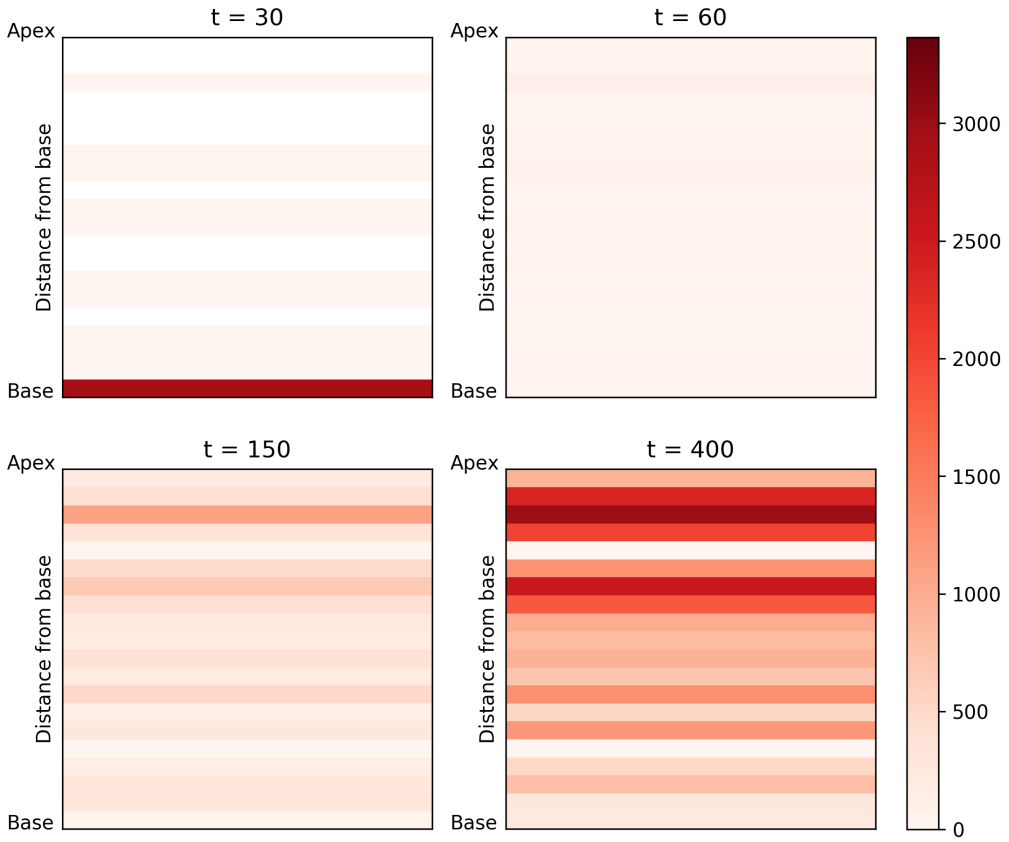

Figure 10: Vertical distribution of average lesion sizes with *TBMetapopPy* simulations during the primary (t=30), early latency (t=60), latency (t=150) and post-primary (t=400) infection stages.

Output	Description
Ω_T	The total number of bacteria (of all states) present within the system
Ω_N	The total number of lesions present within the system (i.e. patches where bacteria count > 0, does not include lesions which have been sterilised)
Ω_S	The average size of all lesions within the system (i.e. the average number of bacteria per patch, includes patches where the lesion has been sterilised)

Table 5: Outputs from *TBMetapopPy* used for sensitivity analysis

results in Figure 10: the reduced perfusion towards the apex improves the chances of bacterial growth in that region, but the perfusion at the very apex is too low to permit the bacteria access to the uppermost region. These factors of interactions and non-linearities mean that in order to perform a valid sensitivity analysis, a global approach must be used, i.e. all parameters must be varied at the same time [38], and the whole n-dimensional (where n is the number of parameters) parameter space must be explored.

In order to do this, we chose to follow the methodology laid out by Marino et al in performing global uncertainty and sensitivity analysis of systems biology models [39]. For our parameter value ranges, where parameters were derived from values from the literature, we assigned a range based on a normal distribution using the literature value as the mean and an appropriate standard deviation value. For parameters which have been estimated, a uniform distribution was chosen with a large range to reflect the additional uncertainty.

There exists a large number of possible outputs from the model. For the purposes of our analysis, we examined three outputs, as listed in Table 5. These values vary over time, as the system moves between different stages of infection. Therefore, we track the sensitivity values of each parameter and output combination over a time period, chosen as being day 1 of infection to day 120 (by which time the primary infection has been contained and a latent infection established). We chose to only perform sensitivity analyses on the primary and latency stages of infection: our model of post-primary disease requires one of the parameters (α_T) to be changed during simulation. The sensitivity analyses we have outlined in this chapter are unable to account for changing parameter values so would not generate accurate results for a post-primary stage.

4.1. PRCC

We began by first calculating Partial Rank Correlation Coefficient (PRCC) values for all parameters against all output variables over the time-span of 120 days. We chose to use 100 stratifications of the input parameter ranges, and used the average results of 20 repetitions in order to reduce the contribution of aleatory uncertainty.

We first plotted the results of our three outcomes in order to perform our Uncertainty Analysis and understand how uncertain our outcomes were. These are shown in Figure 11, which shows the plots of each of the 100 aggregations of 20 repetitions for each parameter sample generated by a Latin Hypercube Sampling method, and summarised in Figure 12, which shows the mean and standard deviation over time of these outputs.

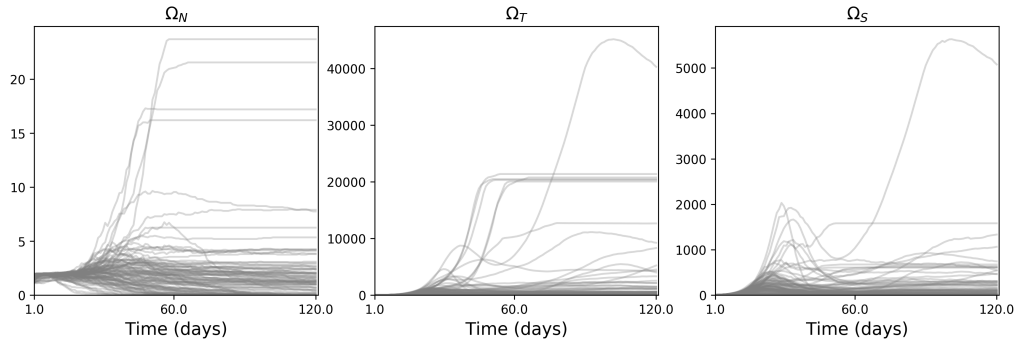

Figure 11: Uncertainty analysis plot of each output over time from each of the 100 averages (of 20 repetitions) for each parameter sample

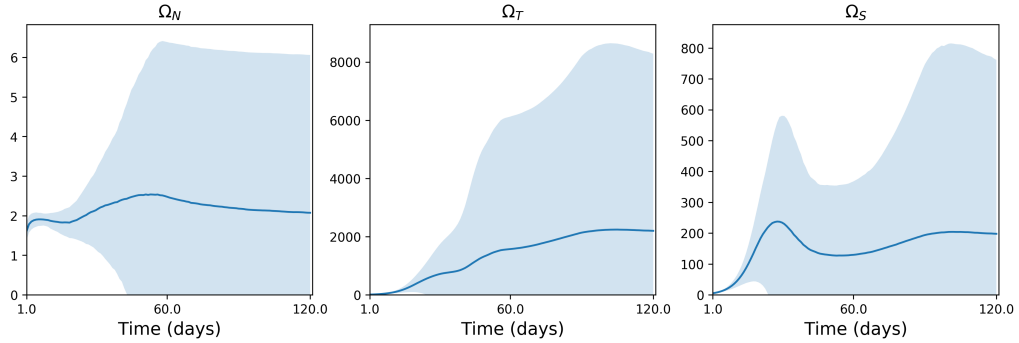

Figure 12: Uncertainty analysis summary statistics plot of all outputs over time from each of the 100 averages (of 20 repetitions) for each parameter sample.

From these plots, we note that there is a high degree of uncertainty in our output variables, particularly in the later stages of infection (as seen by the large errors present for all three outputs in Figure 12. From Figure 11, we see the effects of aleatory and epistemic uncertainty: changes in the model parameters can lead to different scenarios in the outcomes (evidenced by the grouping of results at time t=120.0, particularly for Ω_S and Ω_T), while aleatory uncertainty creates minor fluctuations within these outcomes.

Having established the uncertainty within our model outcomes, we then generated PRCC values for each parameter and output combination over the time-scale of the simulations. The full set of plots and significant sensitivities are presented in the Supplementary Materials, and in this section we overview some of these results.

4.1.1. The influence of environmental parameters

The three environmental parameters, S_V, S_Q and S_G, all exhibit differing sensitivities upon the outputs (see Figure 13). For these variables, an increases indicates a increase in the heterogeneity within the lung; for example, a greater S_V value results in more ventilation being

directed towards the base of the lung and less towards the apex, and similarly for S_Q and S_G. For the number of lesions, the environmental parameters show little sensitivity, with increased drainage at the base showing a slight negative PRCC value during the early stage of infection, implying that better movement of immune cells to the lymphatics can reduce the number of lesions during the primary stage, but this reduces as latency is established. The sensitivity of the S_Q and S_V have little impact on the number of lesions throughout the infection.

After a period of around 30 days, the PRCC values for S_Q against both the total number of

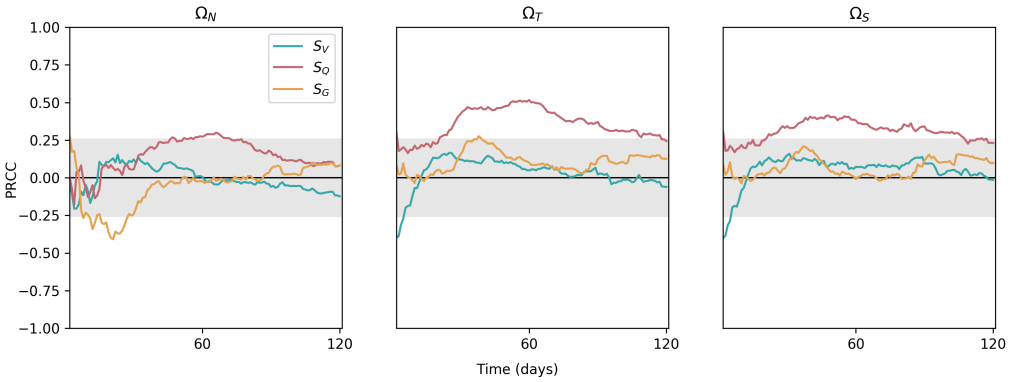

Figure 13: Sensitivity plots for environmental parameters within *TBMetapopPy*, plotting the PRCC value of each parameter against one of the three outputs over time. Grey shaded area shows non-significance (p<0.01).

bacteria and the average lesion size become significant. This implies that the differential in perfusion across the lung has little impact on the primary infection, but does impact the conditions present during latent infection, with a greater differential increasing both the total bacteria present within the patient and the size of the lesions they have developed.

4.1.2. The importance of T cells

Figure 14 shows a selection of the sensitivities of parameters related to T cells against the outputs of the model. We note that the model is highly sensitive to many of these parameters, indicating that T cells play a very important role in the course of infection. For the number of lesions, the sensitivities for most parameters remain in the insignificant range, but for most these values become significant after the primary stage of infection. T cell activation is very important, with ϵ_T having negative values (as greater rates of activation decrease the number of lesions) and $\theta_{\epsilon T}$ having negative values (as an increased half-sat reduces the rate of contact between T cells and antigen-presenting cells). This trend for T cell activation also occurs for the other two outputs. The speed at which T cells destroy macrophages and the contact rates allowing this to occur have high sensitivities for all three outputs, indicating this is an important process to maintain control over infection. Establishing a sufficient T cell presence is also an important factor, with T cell replication have a strongly negative PRCC value, as the proliferation of T cells is necessary in the model to fight bacterial growth.

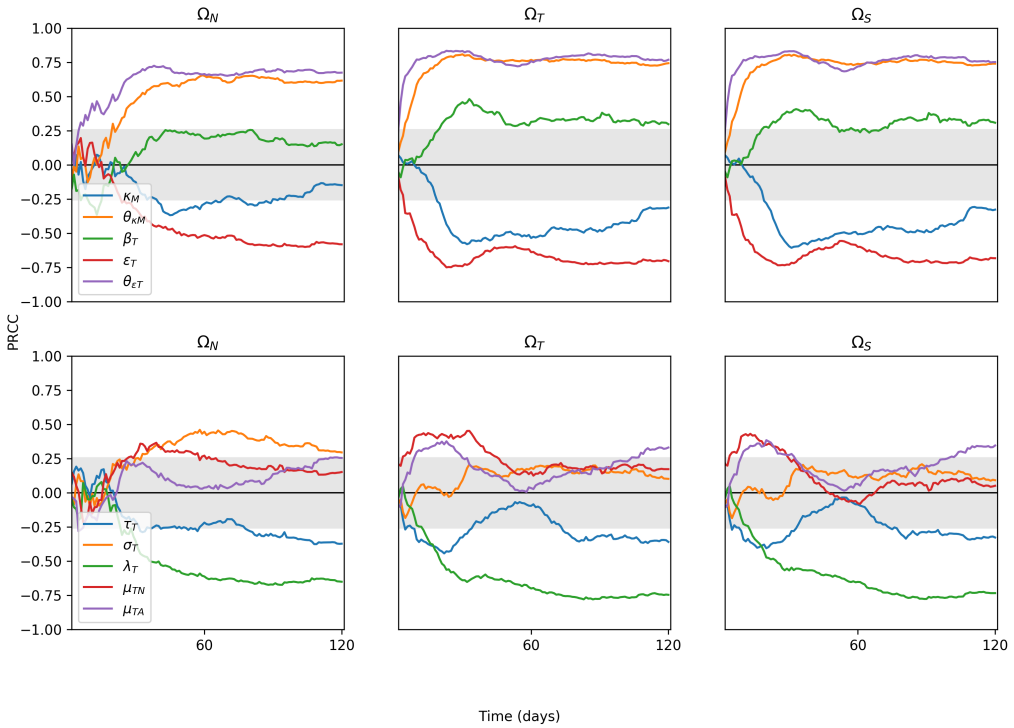

Figure 14: Sensitivity plots for T cell related parameters within *TBMetapopPy*, plotting the PRCC value of each parameter against one of the three outputs over time. Grey shaded area shows non-significance (p<0.01). Only parameters with sustained significant PRCC values against one output are displayed.

4.1.3. Bacterial replication

Our PRCC results show contrasting findings for the replication of intracellular and extracellular bacteria on the outputs, as shown in Figure 15. Intracellular replication (λ_I) has a positive PRCC value for all three outputs during the initial primary infection (albeit with non-significance for Ω_N). This value becomes negative and remains non-significant until briefly becoming significant for all three outcomes at around 30 days. This is in contrast to the two extracellular replication rates, which at 60 days are both positive. This suggests there may be some benefit to bacteria by growing slower when intracellular, possibly due to slower growth reducing the rate of cell death of the macrophage, and thus keeping the bacteria in an environment where they cannot be harmed for a longer period of time.

4.1.4. Translocation of macrophages is more important than translocation of dendritic cells

One perhaps surprising result is that the translocation of macrophages (τ_M) had higher PRCC value than translocation of dendritic cells (τ_D) for most of the time-frame of infection, as shown in Figure 16. τ_M occurs at a much lower rate than τ_D in our model (1e-4 - 1e-1 compared to 0.1 - 1.0 ranges respectively), indicating that this process is an important part bacterial containment within our model, possibly as the macrophages carry a larger quantity of bacteria than the dendritic cells, and thus draining more of them to the lymph nodes and exposing them to activated

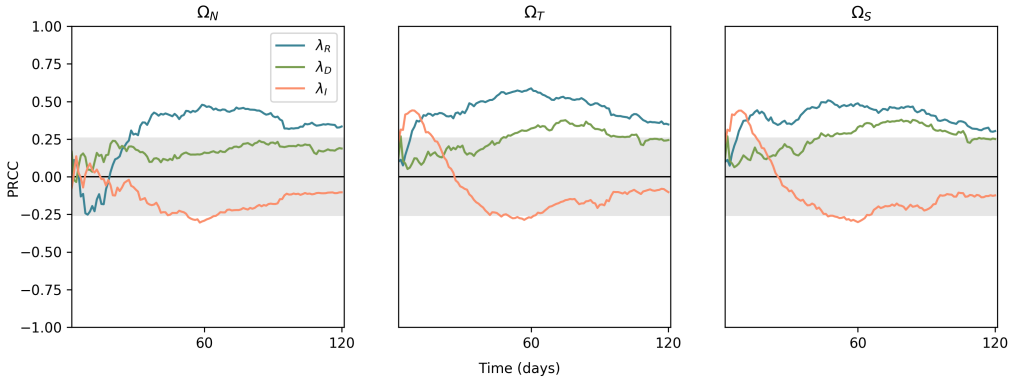

Figure 15: Sensitivity plots for bacterial replication parameters within *TBMetapopPy*, plotting the PRCC value of each parameter against one of the three outputs over time. Grey shaded area shows non-significance (p<0.01).

T cells faster is a suitable mechanism to improve the fight against the bacteria proliferation.

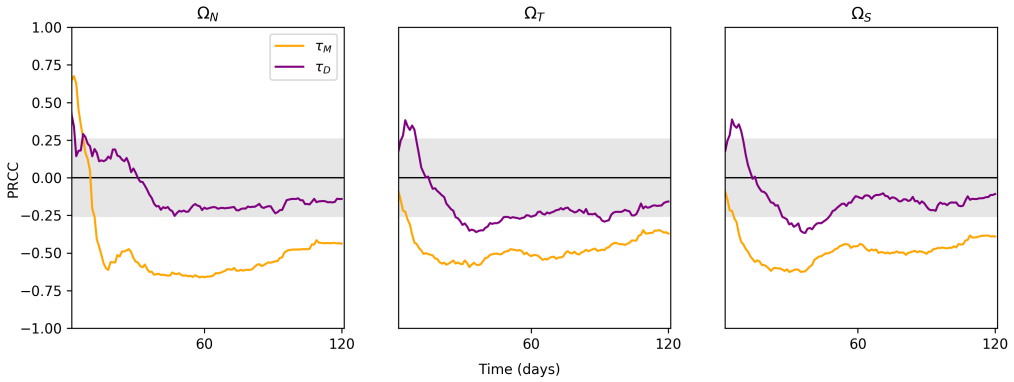

Figure 16: Sensitivity plots for immune cell migration parameters within *TBMetapopPy*, plotting the PRCC value of each parameter against one of the three outputs over time. Grey shaded area shows non-significance (p<0.01).

4.1.5. Parameters affecting different stages

As noted, many parameters within *TBMetapopPy* change significance over time, with some of these corresponding to different stages of infection. Tables A1, A2 and A3 in Supplementary Materials show the effects of all parameters with a significant PRCC against each outcome, stratified into 10 days periods. We see that some parameters that are significant during the first 30 days (i.e. the primary stage of infection) lose significance at later stages. And conversely, parameters that are insignificant during the early stages gain significance later in the simulated time. Examples of this include the rate of death of naïve T cells (μ_{TN}), where increased T cell death results in great bacterial numbers, but only during the primary infection, and enhanced recruitment of macrophages to the lymph nodes (β_{MY}), whereby increased cell recruitment there decreases the average size of lesions and the total number of bacteria within the model, but only from day 51 onwards.

5. Discussion

Computational models of the within-host dynamics of TB have been used extensively to improve our understanding of how disease progresses within the body, particularly at the scale of a single lesion [16, 17, 18] and with some models looking at the disease over the whole lung and the associated lymph nodes [34, 35, 40, 41]. However, these models have not included the notions of heterogeneity of environmental conditions within the lung as shown in this paper, which are believed to be critical to the apical localisation of TB during the crucial post-primary stage [11]. In our first model [19], we presented the first *in silico* model of a pulmonary TB infection that included environmental heterogeneity and bacterial dissemination to show how the environmental conditions at the apex of the lung can favour bacterial growth and lead to larger bacterial loads at that location during latency. In this work, we have expanded on that initial model by including the whole life-cycle, from initial infection with bacteria to post-primary disease.

The results of our numerical simulations have shown that the plausibility of the environmental heterogeneity being the driving factor for a post-primary apical disease localisation within the lung. Within our model, we have set the initial infection to begin in the lower regions of the lungs. As this progresses, the bacteria proliferate until their numbers are brought under control by the adaptive immune response. However, in order to trigger this adaptive response, antigen-presenting cells (dendritic cells and macrophages in our model) must traffic to the draining lymph nodes. By doing so, these cells present a means of bacterial dissemination, since any alive bacteria inside the cells are transferred along with the cell. This establishes a secondary infection within the lymphatic system. There is then a short window in our model whereby bacteria are present in the lymph nodes but before a solid granuloma has formed there, and it is during this period that the free bacteria are able to access the blood stream and re-seed the lung. Various smaller lesions form, but due to the adaptive immune response already being established, these lesions do not reach the sizes of the single lesion seen in the initial infection. These lesions are heterogeneous, with lesions towards the apex reaching a greater size than those lower down. This scale is not completely linear: the regions at the very apex of the lung are so poorly perfused that bacteria cannot reach them. Thus there exists a ideal region, slightly below the apex, where conditions are ideal for bacterial growth. Once an external event reduces the immune response (by knocking out some of the recruitment of T cells), the numerous lesions present begin to expand, and it is in this region that the lesions reach the dangerous sizes seen during primary infection. It would be interesting to make a comparison between the apical location identified in this paper with radiological lesions, but such a study was beyond the scope of this work.

Our sensitivity analysis shows that the skew of perfusion values has a significant effect on the total number of bacteria and the average lesion size during the primary and latency stages, whereas the skews of ventilation and drainage have limited impact. Therefore, we can interpret this as showing that the heterogeneity of perfusion may be the main environmental factor that contributes to the apical localisation, probably due to the reduced immune response it causes there. Differentials in blood flow have long thought to contribute to this apical localisation, with bed rest (which alters the scale and direction of blood flow due to the change in the host's posture [42]) previously being shown to have positive effects on TB recovery [14] and this is the first modelling evidence to support this idea.

The results of our sensitivity analysis also highlight other mechanisms that may contribute to disease outcome. We have demonstrated the importance of T cells within the model, as the majority of T cell related parameters had significant influence on all three of our disease outputs.

For our model, extracellular replication has a greater impact on disease outputs during the latency stage than intracellular replication. Thus, it may be more important to focus treatments on destroying these extracellular bacteria than those in the intracellular niche to improve treatment during latency.

Our *TBMetapopPy* environment models a single individual, with environmental attributes determined at the beginning of simulation remaining constant throughout. In reality, whilst the environment of the lung affects the disease, the reverse is also true, with the disease altering the anatomy of the lung, with tissue destruction and cavitation creating new routes of bacterial dissemination. Furthermore, our model simulates a single individual, with one set of environmental parameters being used for all simulations. However, no two human beings have the same lung, as lung morphology and physiology are affected by a number of factors, including height and body size [43], and sex [44, 45, 46]. Gender may be of particular interest to TB researchers, as there has been shown to be gender differences in responses to treatment: an analysis of the REMoxTB clinical trial revealed that men with cavitation showed poorer response to treatment than women with or without cavitation [47]. These differentials in disease outcome between genders may be caused by biological sex differences between male and female lung morphologies [44, 48], although the causes may also be socio-economic or cultural [49].

The focus of our model has been to simulate the disease in its untreated form. However, it is reasonable to assume that environmental heterogeneities also impact the pharmacokinetics of TB treatment, as all drugs will enter the environment via the blood and thus perfusion differentials may result in inadequate concentrations of chemotherapy reaching the areas of worst bacterial growth. The pharmacodynamics of the different drugs that are currently used to fight TB are affected by different environments and so a variety of different drugs could be included in the model that perform different actions dependent on their location. The ability to combine a whole-organ model of various lung morphologies with a range of possible treatment regimens would confer the ability to create 'virtual clinical trials', where new regimens could be trialled on synthetic patients first, allowing us to make predictions on their likely efficacy and thus better prioritise the regimens to be put into actual trials.

Acknowledgements

This work was supported by the PreDiCT-TB consortium (IMI Joint undertaking grant agreement number 115337, resources of which are composed of financial contribution from the European Unions Seventh Framework Programme (FP7/2007-2013) and EF-PIA companies in kind contribution.

References

[1] World Health Organization, Global Tuberculosis Report 2018 (2018).

[2] S. A. Munro, S. A. Lewin, H. J. Smith, M. E. Engel, A. Fretheim, J. Volmink, Patient Adherence to Tuberculosis Treatment: A Systematic Review of Qualitative Research, PLoS Medicine 4 (7) (2007) e238. doi:10.1371/journal.pmed.0040238.
URL http://www.plosmedicine.org/article/info:doi/10.1371/journal.pmed.0040238

[3] M. Lipsitch, B. R. Levin, Population dynamics of tuberculosis treatment: Mathematical models of the roles of non-compliance and bacterial heterogeneity in the evolution of drug resistance (1998).

[4] S. H. Gillespie, Evolution of drug resistance in Mycobacterium tuberculosis: clinical and molecular perspective, Antimicrobial agents and chemotherapy 46 (2) (2002) 267–274. doi:10.1128/AAC.46.2.267.

[5] E. L. Nuermberger, T. Yoshimatsu, S. Tyagi, R. J. O'Brien, A. N. Vernon, R. E. Chaisson, W. R. Bishai, J. H. Grosset, Moxifloxacin-containing Regimen Greatly Reduces Time to Culture Conversion in Murine Tuberculosis, American Journal of Respiratory and Critical Care Medicine 169 (3) (2004) 421–426. doi:10.1164/rccm.200310-1380OC.

[6] S. H. Gillespie, A. M. Crook, T. D. McHugh, C. M. Mendel, S. K. Meredith, S. R. Murray, F. Pappas, P. P. Phillips, A. J. Nunn, Four-Month Moxifloxacin-Based Regimens for Drug-Sensitive Tuberculosis, New England Journal of Medicine 371 (17) (2014) 1577–1587. doi:10.1056/NEJMoa1407426.

[7] S. H. Gillespie, The role of moxifloxacin in tuberculosis therapy, European Respiratory Review 25 (139) (2016) 19–28. doi:10.1183/16000617.0085-2015.
URL http://err.ersjournals.com/lookup/doi/10.1183/16000617.0085-2015

[8] B. Prideaux, L. E. Via, M. D. Zimmerman, S. Eum, J. Sarathy, P. O'Brien, C. Chen, F. Kaya, D. M. Weiner, P.-Y. Chen, T. Song, M. Lee, T. S. Shim, J. S. Cho, W. Kim, S. N. Cho, K. N. Olivier, C. E. Barry, V. Dartois, The association between sterilizing activity and drug distribution into tuberculosis lesions, Nature Medicine 21 (10) (2015). doi:10.1038/nm.3937.

[9] E. Guirado, L. S. Schlesinger, Modeling the Mycobacterium tuberculosis granuloma - the critical battlefield in host immunity and disease., Frontiers in immunology 4 (April) (2013) 98. doi:10.3389/fimmu.2013.00098.

[10] S. Ahmad, Pathogenesis, immunology, and diagnosis of latent mycobacterium tuberculosis infection, Clinical and Developmental Immunology 2011 (2011). arXiv:814943, doi:10.1155/2011/814943.

[11] P. T. Elkington, J. S. Friedland, Permutations of time and place in tuberculosis, The Lancet Infectious Diseases 15 (11) (2015) 1357–1360. doi:10.1016/S1473-3099(15)00135-8.

[12] V. Balasubramanian, E. Wiegeshaus, B. Taylor, D. Smith, Pathogenesis of tuberculosis: pathway to apical localization, Tubercle and Lung Disease 75 (3) (1994) 168–178. doi:10.1016/0962-8479(94)90002-7.

[13] R. A. Goodwin, R. M. Des Prez, Apical Localization of Pulmonary Tuberculosis, Chronic Pulmonary Histoplasmosis and Progressive Massive Fibrosis of the Lung, Chest 83 (5) (1983) 801–805.

[14] J. F. Murray, Bill Dock and the Location of Pulmonary Tuberculosis: How Bed Rest Might Have Helped Consumption, American Journal of Respiratory and Critical Care Medicine 168 (9) (2003) 1029–1033. doi:10.1164/rccm.200307-1016OE.

[15] R. L. Hunter, J. K. Actor, S. A. Hwang, V. Karev, C. Jagannath, Pathogenesis of post primary tuberculosis: Immunity and hypersensitivity in the development of cavities, Annals of Clinical and Laboratory Science 44 (4) (2014) 365–387.

[16] R. Bowness, M. A. Chaplain, G. G. Powathil, S. H. Gillespie, Modelling the effects of bacterial cell state and spatial location on tuberculosis treatment: Insights from a hybrid multiscale cellular automaton model, Journal of Theoretical Biology 446 (2018) 87–100. doi:10.1016/j.jtbi.2018.03.006.

[17] J. L. Segovia-Juarez, S. Ganguli, D. Kirschner, Identifying control mechanisms of granuloma formation during M. tuberculosis infection using an agent-based model, Journal of Theoretical Biology 231 (3) (2004) 357–376. doi:10.1016/j.jtbi.2004.06.031.

[18] C. L. Sershen, S. J. Plimpton, E. E. May, Oxygen Modulates the Effectiveness of Granuloma Mediated Host Response to Mycobacterium tuberculosis: A Multiscale Computational Biology Approach, Frontiers in Cellular and Infection Microbiology 6 (February) (2016) 1–25. doi:10.3389/fcimb.2016.00006.

[19] M. J. Pitcher, R. Bowness, S. Dobson, S. H. Gillespie, A spatially heterogeneous network-based metapopulation software model applied to the simulation of a pulmonary tuberculosis infection, Applied Network Science 3 (1) (2018) 33. doi:10.1007/s41109-018-0091-2.

[20] R. J. H. Hammond, V. O. Baron, K. Oravcova, S. Lipworth, S. H. Gillespie, Phenotypic resistance in mycobacteria: is it because I am old or fat that I resist you?, Journal of Antimicrobial Chemotherapy 70 (10) (2015) 2823–2827. doi:10.1093/jac/dkv178.

[21] S. Lipworth, R. Hammond, V. Baron, Y. Hu, A. Coates, S. Gillespie, Defining dormancy in mycobacterial disease, Tuberculosis 99 (2016) 131–142. doi:10.1016/j.tube.2016.05.006.

[22] D. G. Russell, H. C. Mwandumba, E. E. Rhoades, Mycobacterium and the coat of many lipids, Journal of Cell Biology 158 (3) (2002) 421–426. doi:10.1083/jcb.200205034.

[23] I. Vergne, J. Chua, S. B. Singh, V. Deretic, Cell biology of mycobacterium tuberculosis phagosome., Annual review of cell and developmental biology 20 (2004) 367–394. doi:10.1146/annurev.cellbio.20.010403.114015.

[24] A. J. Wolf, B. Linas, G. J. Trevejo-Nunez, E. Kincaid, T. Tamura, K. Takatsu, J. D. Ernst, Mycobacterium tuberculosis infects dendritic cells with high frequency and impairs their function in vivo, J Immunol 179 (4) (2007) 2509–2519. doi:179/4/2509 [pii].

[25] E. Giacomini, E. Iona, L. Ferroni, M. Miettinen, L. Fattorini, G. Orefici, I. Julkunen, E. M. Coccia, Infection of human macrophages and dendritic cells with Mycobacterium tuberculosis induces a differential cytokine gene expression that modulates T cell response., Journal of immunology (Baltimore, Md. : 1950) 166 (12) (2001) 7033–7041. doi:10.4049/jimmunol.166.12.7033.

[26] I. E. A. Flesch, S. H. E. Kaufmann, Activation of tuberculostatic macrophage functions by gamma interferon,

interleukin-4, and tumor necrosis factor, Infection and Immunity 58 (8) (1990) 2675–2677.
[27] J. L. Flynn, J. Chan, Immunology of Tuberculosis, Annual Review of Immunology 19 (1) (2001) 93–129. doi:10.1146/annurev.immunol.19.1.93.
[28] P. L. Lin, J. L. Flynn, CD8 T cells and Mycobacterium tuberculosis infection, Seminars in Immunopathology 37 (3) (2015) 239–249. doi:10.1007/s00281-015-0490-8.
[29] J. B. West, Ventilation-Perfusion Relationships, in: Respiratory Physiology: The Essentials, 7th Edition, Lippincott Williams & Wilkins, Baltimore, Maryland, USA, 2005, Ch. 5, pp. 55–74.
[30] D. Alvarez, E. H. Vollmann, U. H. von Andrian, Mechanisms and Consequences of Dendritic Cell Migration, Immunity 29 (3) (2008) 325–342. doi:10.1016/j.immuni.2008.08.006.
[31] A. Mihret, The role of dendritic cells in Mycobacterium tuberculosis infection., Virulence 3 (7) (2012) 654–9. doi:10.4161/viru.22586.
[32] A. C. Kirby, M. C. Coles, P. M. Kaye, Alveolar Macrophages Transport Pathogens to Lung Draining Lymph Nodes, The Journal of Immunology 183 (3) (2009) 1983–1989. doi:10.4049/jimmunol.0901089.
[33] A. J. Wolf, L. Desvignes, B. Linas, N. Banaiee, T. Tamura, K. Takatsu, J. D. Ernst, Initiation of the adaptive immune response to Mycobacterium tuberculosis depends on antigen production in the local lymph node, not the lungs., The Journal of experimental medicine 205 (1) (2008) 105–15. doi:10.1084/jem.20071367.
[34] S. Marino, D. E. Kirschner, The human immune response to Mycobacterium tuberculosis in lung and lymph node., Journal of Theoretical Biology 227 (4) (2004) 463–486. doi:10.1016/j.jtbi.2003.11.023.
[35] S. Marino, A. Myers, J. L. Flynn, D. E. Kirschner, TNF and IL-10 are major factors in modulation of the phagocytic cell environment in lung and lymph node in tuberculosis: A next-generation two-compartmental model, Journal of Theoretical Biology 265 (4) (2010) 586–598. doi:10.1016/j.jtbi.2010.05.012.
[36] L. L. Roberts, C. M. Robinson, Mycobacterium tuberculosis infection of human dendritic cells decreases integrin expression, adhesion and migration to chemokines, Immunology 141 (1) (2014) 39–51. doi:10.1111/imm.12164.
[37] K. C. Stone, R. R. Mercer, P. Gehr, B. Stockstill, J. D. Crapo, Allometric relationships of cell numbers and size in the mammalian lung., American journal of respiratory cell and molecular biology 6 (2) (1992) 235–243. doi:10.1165/ajrcmb/6.2.235.
[38] A. Saltelli, K. Aleksankina, W. Becker, P. Fennell, F. Ferretti, N. Holst, S. Li, Q. Wu, Why so many published sensitivity analyses are false: A systematic review of sensitivity analysis practices, Environmental Modelling and Software 114 (March 2018) (2019) 29–39. doi:10.1016/j.envsoft.2019.01.012.
[39] S. Marino, I. B. Hogue, C. J. Ray, D. E. Kirschner, A methodology for performing global uncertainty and sensitivity analysis in systems biology, J Theor Biol 254 (1) (2008) 178–196. doi:10.1016/j.jtbi.2008.04.011.
[40] J. E. Wigginton, D. Kirschner, A model to predict cell-mediated immune regulatory mechanisms during human infection with Mycobacterium tuberculosis., Journal of Immunology 166 (3) (2001) 1951–67. doi:10.4049/jimmunol.166.3.1951.
[41] G. Magombedze, W. Garira, E. Mwenje, Modelling the human immune response mechanisms to mycobacterium tuberculosis infection in the lungs, Math Biosci Eng 3 (3) (2006) 661–682. doi:10.3934/mbe.2006.3.661.
[42] I. Galvin, G. B. Drummond, M. Nirmalan, Distribution of blood flow and ventilation in the lung: Gravity is not the only factor, British Journal of Anaesthesia 98 (4) (2007) 420–428. doi:10.1093/bja/aem036.
[43] C. D. Cook, P. J. Helliesen, S. Agathon, Relation Between Mechanics of Respiration, Lung Size and Body Size From Birth to Young Adulthood, Journal of Applied Physiology 13 (3) (1958) 349–352. doi:10.1152/jappl.1958.13.3.349.
[44] J. Cohen, W. R. Douma, N. H. ten Hacken, M. Oudkerk, D. S. Postma, Physiology of the small airways: A gender difference?, Respiratory Medicine 102 (9) (2008) 1264–1271. doi:10.1016/j.rmed.2008.04.007.
[45] E. A. Townsend, V. M. Miller, Y. S. Prakash, Sex differences and sex steroids in lung health and disease, Endocrine Reviews 33 (1) (2012) 1–47. doi:10.1210/er.2010-0031.
[46] M. R. Becklake, F. Kauffmann, Gender differences in airway behaviour over the human life span, Thorax 54 (12) (1999) 1119–1138. doi:10.1136/thx.54.12.1119.
[47] M. E. Murphy, G. H. Wills, S. Murthy, C. Louw, A. L. C. Bateson, R. D. Hunt, T. D. McHugh, A. J. Nunn, S. K. Meredith, C. M. Mendel, M. Spigelman, A. M. Crook, S. H. Gillespie, Gender differences in tuberculosis treatment outcomes: a post hoc analysis of the REMoxTB study, BMC Medicine 16 (1) (2018) 189. doi:10.1186/s12916-018-1169-5.
[48] O. Neyrolles, L. Quintana-Murci, Sexual inequality in tuberculosis, PLoS Medicine 6 (12) (2009). doi:10.1371/journal.pmed.1000199.
[49] P. Hudelson, Gender differentials in tuberculosis: The role of socio-economic and cultural factors, Tubercle and Lung Disease 77 (5) (1996) 391–400. doi:10.1016/S0962-8479(96)90110-0.